Streptavidin binding to biotinylated lipid layers on solid supports

A neutron reflection and surface plasmon optical study

A. Schmidt,* J. Spinke,* T. Bayerl,‡ E. Sackmann,‡ and W. Knoll*§

*Max Planck Institut für Polymerforschung, W-6500 Mainz, Germany; and ‡Physik Department E 22, Technische Universität München, W-8046 Garching, Germany

ABSTRACT Neutron reflection and surface plasmon optical experiments have been performed to evaluate structural data of the interfacial binding reaction between the protein streptavidin and a solid-supported lipid monolayer partly functionalized by biotin moieties. Since both experimental techniques operate in a total internal reflection geometry at a substrate/solution interface, identical sample architectures allow for a direct comparison between the results obtained with these two recently developed methods. It is found that a monomolecular layer of dipalmitoyllecithin doped with 5 mol% of a biotinylated-phosphatidylethanolamin shows a thickness of $d_1 \approx (3.4 \pm 0.5)$ nm.

Binding of streptavidin to the biotin groups results in an overall layer thickness of $d = (5.9 + 0.5)$ nm that demonstrates the formation of a well-ordered protein monolayer with the (biotin + spacer) units of the functionalized lipids being fully embedded into the binding pocket of the proteins. It is demonstrated by model calculations that a more detailed picture of the internal structure of this supramolecular assembly can only be obtained if one uses deuterated lipid molecules, thus generating a high contrast between individual layers.

INTRODUCTION

Specific binding reactions between biotin (vitamin H) and the tetrameric protein streptavidin are well characterized in solution (1) and are widely used in biodiagnostic assays (2). Only recently, however, these systems also attracted a great deal of interest as a model for the study of recognition reactions between a ligand and a receptor at highly-organized surfaces (3–9). Biotin can be easily bound, e.g., to the headgroup of lipid molecules (3), thus allowing for the preparation of functionalized monomolecular layers at the water-air interface. Binding of streptavidin can then be observed by optical techniques like ellipsometry (10, Reiter, R., Motschmann, H., and Knoll, W., manuscript in preparation) or fluorescence microscopy (3, 6) (provided, of course, the protein is correspondingly labeled by a chromophore) or by x-ray and neutron reflection techniques (11).

For the functionalization of solid interfaces in contact with an aqueous phase, two different approaches have been taken. The first involves the synthesis of long-chain thiols with biotin residues in the ω-position which then can be organized in a self-assembly process to build a monomolecular layer covering an Ag or Au substrate (8). It has been shown that these interfaces can have a high binding affinity for streptavidin if one carefully engineers the molecular structure, the site density, relative orientational constraints, etc. (12).

A second way uses the so-called Langmuir-Blodgett-Kuhn (LBK) technique (13): a functionalized monomolecular layer is prepared at the water/air interface by spreading a lipid solution in a volatile solvent and subsequently compressing the amphiphilic molecules to the desired lateral density. In this way, monolayers in different physical states, corresponding to, e.g., a liquid-expanded or solid-condensed phase, can be prepared. By a simple dipping procedure, such a monolayer can be transferred to a hydrophobic substrate in a tail-down configuration. If kept permanently in contact with the aqueous subphase, then this layer can form a stable coating of the solid surface with biotin-binding sites exposed to the solution within a matrix with membrane-like properties (6).

For a detailed analysis of interfacial recognition and binding reactions, e.g., in terms of the binding affinity, capacity, kinetics, reactivity, et cetera, it is important to have the full control of the supramolecular architecture at the molecular level. Since one is dealing typically with only a few layers in a complex structured but ultrathin sample at a solid support in contact with an aqueous solution, there are not that many experimental techniques available that are sensitive enough to be helpful.

It is the aim of the present paper to directly compare two of these methods, i.e., surface plasmon (SP) spectroscopy (14) and neutron reflection (15). Both techniques operate in a total internal reflection geometry, thus allowing for the use of identical sample configurations for this comparison, although, of course, different physical quantities of the supramolecular layers are probed: while in the optical case the optical thicknesses, i.e., the geometrical thicknesses of the sublayers, deconvoluted in a certain way with the optical indices of refraction n_{oi} of the individual layers (16), are obtained, neutron reflectivity data taken as a function of the angle of incidence near the cut-off angle for total internal reflection yield thickness data of the interfacial layers convoluted with their respective scattering length densities which can also be expressed in terms of effective (neutron) indices of re-

Address correspondence to Dr. Knoll.

§ W. Knoll is now with The Institute of Physical and Chemical Research (RIKEN), Frontier Research Program, 2-1 Hirosawa, Wako, Saitama 351-01, Japan.

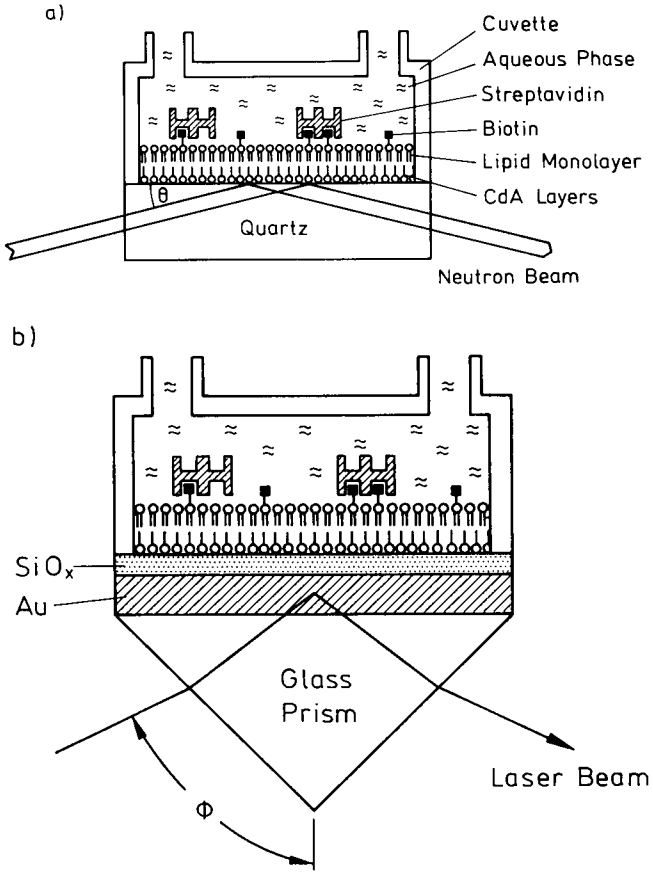

FIGURE 1 (*a*) Schematic of the sample configuration used for neutron measurements in total internal reflection geometry at a solid-solution interface. A thick quartz plate is coated with three layers of CdA (for simplicity, only one layer of CdA is drawn schematically) and a top layer of DPPC doped with biotinylated lipid (5 mol%) facing the aqueous volume of a cuvette. Injected streptavidin can bind from solution to the recognition sites biotin. (*b*) The equivalent sample configuration adapted for surface plasmon experiments in total internal reflection at the base of a glass prism. First, a thin layer of Au ($d \simeq 45$ nm) was evaporation deposited onto which SiO_x ($d \simeq 5$ nm) was evaporated to obtain a clean hydrophilic surface comparable with the quartz substrate used for neutron reflection experiments. All other details of the sample configuration as in *a*.

fraction, n_{ni} (see below). Information about the internal structure of the various layers can be obtained only if a sufficient difference between their respective indices of refraction (≡ contrast) is given. This is typically not the case for the light optical experiments but is a particularly promising feature of neutron reflectivity studies with the possibility to manipulate this contrast by selective deuteration of individual layers.

The sample architecture used in this study to evaluate the diagnostic value of the two experimental approaches was prepared by the LBK technique.

EXPERIMENTAL

Neutron reflectivity measurements

Fig. 1 *a* sketches schematically the sample cell configuration used for the neutron reflectivity measurements. A thick ($d_1 \approx 1$ cm) polished quartz plate (10×5 cm^2) is used as substrate for the LBK multilayer preparation (see below). After the last functionalized lipid monolayer is deposited by a near horizontal dipping in the Langmuir-trough, the top of the cuvette is mounted under water, thus, allowing for a transfer of the cell into the neutron spectrometer with the sample remaining in a stable configuration. Inlet and outlet of the cell cover can be used for the exchange of the subphase, e.g., against streptavidin containing solution or against D_2O buffer.

Reflected intensities were taken from 0.1° up to ~1.8°, thus covering, in particular, the angular range of the total internal reflection. Details of the spectrometer TOREMA are described elsewhere (17).

The wavelength $\lambda = 0.43$ nm is fixed by a graphite monochromator. The flux on the sample amounts to 100,000 neutrons/cm^2 s and can be attenuated by different poly(methylmethacrylate) plates to protect the position sensitive proportional He-3 counter (ORDELA/Oak Ridge, USA). This linear detector allows for a resolution of $\Delta\theta = 0.005°$. The neutron beam is collimated to 0.6 mm width, 1.0 cm height, and a divergence angle of 0.02°.

The sample is rotated in steps of 0.01°, and the reflected intensity is detected. The whole measurement takes ~12 h. The intensity is normalized to the incoming intensity and corrected for the background, which is obtained simultaneously by the linear detector.

The so defined reflectivity R is compared with simulations of different models, calculated with the Fresnel matrix method (18) until the two curves correspond. The models are determined by the index of refraction $n_n(z)$ as a function of depth z. Here, the refractive index depends linearly on the scattering length density ρ of the different compounds of the sample $n_n = 1 - \rho\lambda^2/2\pi$.

It was found that the quartz cannot be described with a simple box model, smeared by an error function transition to the organic layers. Instead, on top of the bulk quartz a 7.8-nm-thick layer with a 15% reduced scattering length density has to be introduced. This surface layer is a result of the polishing procedure.

Surface plasmon spectroscopy

Fig. 1 *b* shows schematically the setup for SP spectroscopic evaluation of the LBK films at a solid/solution interface. The drawing is scaled so as to match the dimensions of the equivalent configuration for neutron reflectivity shown in Fig. 1 *a*.

The Au-film ($d \approx 45$ nm) required for surface plasmon (plasmon surface polariton or SP for short) excitation in this Kretschmann configuration (19) is evaporated onto a glass slide (LaSFN9, $n = 1.85$ at $\lambda = 633$ nm; Schott Glas AG, Mainz, Germany) and subsequently coated with a thin SiO_x layer to get a hydrophilic surface suitable for LBK layer deposition in the identical architecture as prepared for the neutron experiments. Details of the substrate preparation and the experiments are described in references 6, 8, 12, and 15. Again, after the final layer was deposited in a tail-down configuration, the top part of the flow cuvette was mounted under water and the whole cell integrated into the SP-spectrometer (6). The prism (also LaSFN9-glass) needed as plasmon-coupler was attached by refractive-index matching fluid, and the reflected intensity coming from a HeNe laser ($\lambda = 633$ nm, $P = 5$ mW, Uniphase Inc., Sunnyvale, CA) was recorded as a function of the angle of incidence. The characteristic dips in the reflectivity curves were analyzed by Fresnel calculations describing the different layers by box models with a given index of refraction and geometrical thickness. The error of the thickness determination is ±0.5 nm. For details of this experimental approach and of the fit routines, we refer to the literature (14, 16).

Sample preparation

The quartz plates for the neutron experiments were treated in a plasma cleaner before the LBK-film deposition; the freshly evaporated SiO_x surfaces for the SP spectroscopy were used as taken out of the vacuum system. First, three layers of cadmium arachidate ($((CH_3—(CH_2)_{18}COO^-)_2Cd^{++}$, CdA; Sigma Chemical Co., St. Louis, MO) were

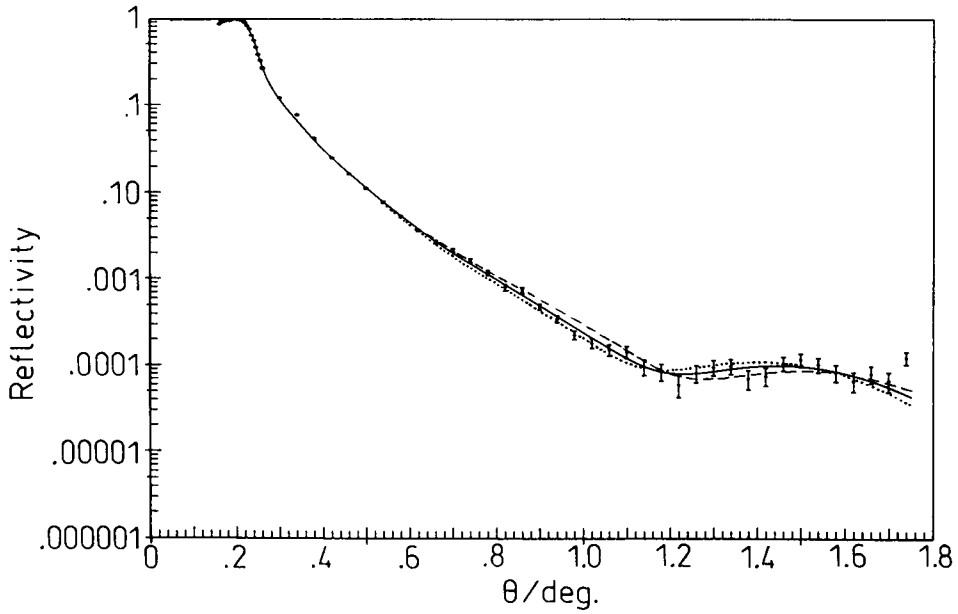

FIGURE 2 Neutron reflectivity data as a function of the angle of incidence θ (see Fig. 1 *a*) obtained for the sample architecture: quartz/three layers CdA/one monolayer of $DPPC_{0.95}$ Biotin-$DPPE_{0.05}/D_2O$. The bars give the statistical error of the data points. The full curve is a fit calculation with the parameters given in Table 1, in particular with a thickness for the lipid layer of $d_l = 3.7$ nm. The dashed curve is calculated with $d_l = 3.2$ nm and the dotted curve with $d_l = 4.2$ nm.

deposited vertically at a surface pressure of $\pi = 30$ mN/m at $T = 20°C$. For the large quartz plates, a home-build Langmuir-system with "floating-boat" barrier in a correspondingly large glass trough was used. This particular architecture with the CdA as spacer layers was chosen to mimic polymeric buffer layers used in other sample configurations related to "polymer supported bilayers." In addition, it decouples the functionalized target layer from the rigid substrate. The biotinylated lipid monolayer was prepared by cospreading L-α-dipalmitoyl-phosphatidylcholine (DPPC; Fluka Chemie AG, Buchs, Switzerland) with -α-5 mol% of *N*-(6-((biotinoyl)amino)hexanoyl)dipalmitoyl-L-α-phosphatidyl-ethanolamin (biotin-DPPE, obtained from Molecular Probes Inc., Eugene, OR) and compressing the layer to $\sim\pi = 10$ mN/m, which corresponds to a fluid-expanded phase known to be most reactive to protein binding. This then was horizontally deposited onto the quartz (SiO_x)/3 CdA-substrate, and after mounting the cell and exchange of the subphase against D_2O (99.9%; Fluka) first experiments were carried out with these reference layers. Next, the aqueous phase was exchanged against a 5×10^{-7} M streptavidin (kindly provided by Boehringer Mannheim GmbH, Werk Tutzing, Germany) containing solution and the protein allowed to diffuse and bind to its recognition sites during 50 min. After again carefully exchanging the aqueous phase against D_2O, a new set of reflectivity data was taken.

RESULTS AND DISCUSSION

Functionalized lipid layer at a solid/solution interface

Neutron reflectivity data

Fig. 2 shows the neutron reflectivity curve measured between $\theta = 0.2$ deg and $\theta = 1.7$ deg for the sample architecture quartz/3CdA/1biotin-lipid/D_2O. Data points together with their statistical errors are shown. The recorded intensity varies over more than four orders of magnitude with a clearly pronounced interference minimum at $\theta \simeq 1.2$ deg. However, the complex interfacial architecture does not allow one to derive to geometrical data in a direct way from this interference minimum. Instead, to model this multilayer sample and to describe its reflectivity curve, one needs additional information. (*a*) The quartz substrate cannot be described by a single box but instead requires a more complicated scattering length density profile to model its surface region that has different properties than the bulk (cf. the profile used in the simulations discussed below; Fig. 6). This is well documented and was checked independently for our case before any lipid layer deposition. (*b*) The structure of CdA is well known (20). Averaging over the headgroup region and the aliphatic tails, one expects a thickness per monolayer of $d = 2.7$ nm and a scattering length density of $\rho_{CdA} = 1.09 \times 10^{-5}$ nm^{-2} (21). An independent check of the three CdA layers by x-ray reflectivity confirmed the thickness of $d \approx 8.1$ nm (see also the optical data below). (*c*) The averaged scattering length density of the lipid layers is $\rho_{lipid} = 2.51 \times 10^{-5}$ nm^{-2} (22). The fluid DPPC monolayer without biotin-labels is expected to be $d \approx 2.4$ nm thick (21, 23, 24).

Now, the best fit to the experimental data is given in Fig. 2 by the full line. The parameters used are given in Table 1. Shown in Fig. 2 are also reflectivity curves calculated allowing the biotin-lipid layer to vary by +0.5 nm (*dotted curve*) or −0.5 nm (*dashed curve*). Several points are noteworthy with respect to the parameters given in Table 1. (*a*) The scattering length density of the 3CdA layers is considerably higher than expected. This is

TABLE 1 **Fit parameters used to calculate the reflectivity curve that best fits the neutron data obtained for the biotinylated lipid layer before protein adsorption**

Sample architecture	Fit parameters
Quartz	Bulk + surface region*
Three CdA layers	
Thickness d_0 (nm)	8.1 ± 0.5
Scattering length density ρ_{C_dA} (nm^{-2})	$1.74 \cdot 10^{-4}$ (x = 28% D_2O)‡
Interface width§ (nm)	0.2
Biotinylated lipid monolayer	
Thickness d_1 (nm)	3.7 ± 0.5
Scattering length density ρ (nm^{-2})	$2.30 \cdot 10^{-4}$ (x = 35% D_2O)‡
Interface width§ (nm)	0.2
D_2O	
Scattering length density ρ_{D_2O} (nm^{-2})	$6.07 \cdot 10^{-4}$ (x = 95.7% D_2O)‡

* See text and Fig. 6 (Quartz profile used for the simulations). ‡Calculated according to $\rho_{exp} = \rho_{D_2O} \cdot x + \rho_{theoretical} \cdot (1 - x)$. §By the interface layer a smooth transition from one layer to the next is taken into account by an error function.

presumably due to patch defects filled with D_2O. A volume fraction of as much as 28% would explain the scattering length density. This could point to a certain instability of this multilayer configuration during the solvent manipulations in the course of the sample preparation. (*b*) The D_2O volume fraction of the biotin-lipid layer is even higher. But this is conceivable given the bulky polar headgroups of DPPC and biotin-DPPE that are largely hydrated. (*c*) Very remarkable is the somewhat unexpected high value d_1 = 3.7 nm for the thickness of the biotin-lipid layer. As mentioned already, the DPPC monolayer in the fluid phase was found by various authors to be ~2.4 nm thick (21, 23, 24). The biotin moiety amounts to ~1.0 nm, the spacer that links it to the lipid brings another 0.8 nm (if fully extended). The large thickness found by neutron reflectivity, therefore, is not unrealistic and also the high (heavy) water content fits to this estimate. One has to bear in mind, however, that only 5% of the lipid molecules carry a biotin group. Another contribution to both, the high water content and the large thickness, could be that during the transfer the biotin-lipid layer that was certainly fluid expanded on the water surface condenses into crystalline patches of higher thickness at the moment when it is deposited onto the CdA layers. (*d*) The D_2O content of the aqueous medium (x = 95.7%) demonstrates the successful exchange of the subphase after the simple cell preparation.

Surface plasmon measurements

Before any LBK layer deposition, the bare Au substrates and the SiO_x layers were characterized surface plasmon optically. The obtained values for the thickness and the complex dielectric constant of Au (at λ = 633 nm) and the thickness and real dielectric constant for the SiO_x layer (all given in Table 2) were then used for the further Fresnel calculations.

Fig. 3 *a* shows the reflectivity curve (*open circles*) obtained in air after the deposition of three layers of CdA. The dashed curve is calculated assuming for the CdA an index of refraction of n = 1.50 and a thickness of d = 83 Å in excellent agreement with the neutron data and literature values (25).

After the deposition of the biotin-lipid layer now measured in water (hence the different angular range for the SP resonance), an additional layer with a thickness of d = 3.1 nm (assuming n = 1.5 [26] see Table 2) is found (see open data points and dashed curve in Fig. 3 *b*). This result is in agreement with the neutron data, in particular, if one takes into account that the two techniques may average differently over the given scattering length or refractive index profile of the lipid layer.

For comparison with the neutron reflectivity measurements, the same surface plasmon optical experiment was also performed in D_2O. However, no significant difference in the SP excitation was found pointing to an identical lipid layer architecture. In addition, the fluorescence microscopic control experiment with a DPPC-lipid monolayer doped with 5 mol% biotinylated DPPE and bound streptavidin in H_2O showed no major difference of its phase behavior if the subphase was exchanged against D_2O (M. Liley, personal communication). Therefore, most optical experiments were performed in only H_2O buffer.

Streptavidin binding to the biotin-lipid layer

Neutron data

After binding of streptavidin to the lipid layer (and exchange of the protein solution against pure D_2O-buffer) the neutron-reflectivity curve given in Fig. 4 is obtained.

TABLE 2 **Parameters used for the Fresnel calculations performed to fit the SP resonance curves (cf. Figs. 3, *a* and *b*)**

Sample architecture	Fit parameters
LaSFN9 + index fluid	n = 1.846*
Au Layer	
Thickness (nm)	d = 44.7*
Dielectric constant	$\tilde{\epsilon} = 12.0 + i \cdot 1.25$*
SiO_x layer	
Thickness (nm)	d = 4.5*
Index of refraction	n = 1.45*
Three CdA layers	
Thickness (nm)	d_0 = 8.3*
Index of refraction	n = 1.50*
Biotinylated lipid monolayer	
Thickness (nm)	d_1 = 3.1
Index of refraction	n = 1.50
H_2O buffer (0.5 M NaCl)	
Index of refraction	n = 1.336

* Data taken at λ = 633 nm in air.

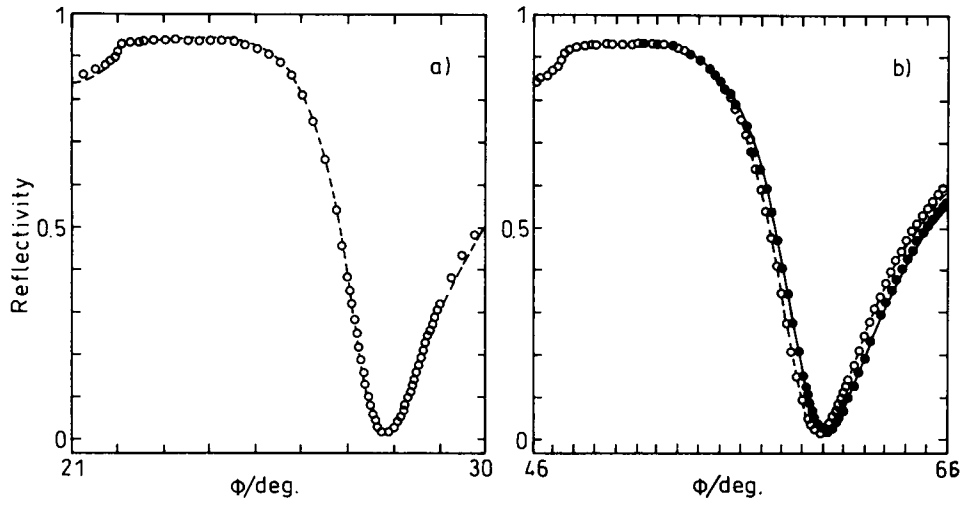

FIGURE 3 (*a*) Surface plasmon optical experiment in air with three layers of CdA deposited onto the Au/SiO_x substrate. The dip in the reflectivity (○) can be well fitted by Fresnel calculations (– – –) with parameters given in Table 2. (*b*) Optical reflectivity data obtained after one monolayer of biotinylated lipid was deposited onto the CdA buffer layers (see *a*) with the headgroups facing the aqueous medium (○). Note the shifted angular range of SP excitation if measured in water. From the Fresnel fit (– – –, parameters given in Table 2), the monolayer thickness is derived. After injection of streptavidin to give a final protein concentration of $c = 5 \times 10^{-7}$ M, the angular position for SP excitation is further shifted to higher values (●). The fit calculations yield an overall thickness increase by the streptavidin layer: $d_2 = 2.8$ nm (——; see also Table 2).

To demonstrate the pronounced effect of protein binding on the reflected intensities, the dashed curve given in Fig. 4 repeats the best fit curve from Fig. 2 obtained before protein injection.

To simulate the new interfacial architecture, a scattering length density for the protein (including the incorporated biotin groups and their spacers) of $\rho_{StA} = 1.231^{-4}$ nm^{-2} was used. With this assumption and keeping the quartz data and the thickness of the CdA layers constant, the scattering length density of these layers has slightly

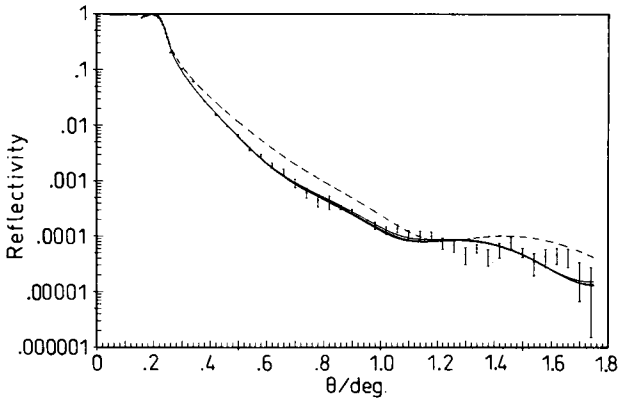

FIGURE 4 Neutron reflectivity data as a function of the angle of incidence θ obtained after binding of a monolayer of streptavidin from solution to the biotin-functionalized substrate. Bars give the statistical error of the data points. The three full curves correspond to Fresnel calculations each performed with a constant thickness for the lipid/protein layer of $d = 5.8$ nm, varying, however, the relative thickness of the lipid layer (1.3, 1.7, and 2.1 nm, respectively). For comparison, the best fit of the reflectivity data from Fig. 2 obtained before protein binding is given as the dashed curve.

increased now corresponding to 38% D_2O, that of the lipid layer to ~43% D_2O, and the protein layer would contain 29% D_2O. The choice for the thickness of the lipid layer without spacer and biotin moieties of $d_1 = 1.7$ nm and for the streptavidin layer of $d_2 = 4.1$ nm was arbitrary and only biased by the known geometrical dimensions of the protein (27). However, what can be obtained by this experiment is the sum over both layer thicknesses corresponding to 5.8 nm. This is demonstrated by the two other calculated reflectivity curves that are almost identical to the "best fit" and would correspond to 1.3/4.5 and 2.1/3.7 nm, respectively.

In a different approach to model the reflection curve, we kept the thickness and the scattering length density of the lipid layer as determined in the absence of the protein ($d_1 = 3.7$ nm) and allowed only the thickness of the protein layer and its scattering length density to be adjusted. This procedure, however, was able to fit the experimental curve less satisfying over the full angular range.

Surface plasmon-optical observation of streptavidin binding

If the identical procedure for protein binding at the biotinylated lipid surface is observed by surface plasmon spectroscopy, the reflectivity curve given also in Fig. 3 *b* (full symbols and full curve) is obtained. From the angular shift of the resonance relative to that of the bare lipid that amonts $\Delta\phi \approx 0.5°$, one calculates a thickness increase by protein binding ($n = 1.45$) (28) of $d = 2.8$ nm. Of course, in this experiment, there is absolutely no possibility to discriminate between the thickness of the lipid layer and that of the protein monolayer. That means that again only the sum of the two layers $d_1 + d_2 = 5.9$ nm is

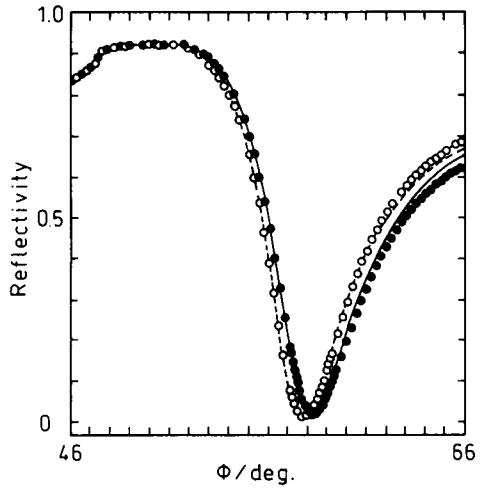

FIGURE 5 Optical reflectivity data obtained for the sample architecture: glass prism/45 nm Au/one layer $DPPC_{0.95}$ Biotin-$DPPE_{0.05}/H_2O$. Data points (O) can be described by a Fresnel curve (– – –), assuming a lipid layer thickness of d_1 = 3.4 nm. After injection of streptavidin (final concentration $c = 5 \times 10^{-7}$ M), the SP resonance is shifted to higher angles (●) and can be fitted by assuming an additional (protein) layer of d_2 = 3.2 nm (——).

obtained. The agreement with the neutron data is very good. Both techniques give a thickness increase upon protein binding which is lower compared with results obtained for other functionalized lipid systems (6, 7).

To rule out that the particular architecture used in this study with the 3 CdA spacer layers whose thickness was kept constant in the analysis would produce an artefact in the protein thickness evaluation, we performed another SP experiment with a different layer preparation. Directly onto the hydrophobic gold surface the biotin-lipid layer was deposited tail-down and mounted into the liquid cell.

The measured reflectivity curve of only the lipid layer is given in Fig. 5 (*open symbols*) together with the fit curve (*dashed curve*) yielding 3.4 nm for the monolayer thickness. This value is again comparable with the value obtained by both techniques in the case with the CdA spacer layers. Now, addition of the same concentration of streptavidin leads again to a thickness increase by irreversible binding of Δd = 3.2 nm (*full symbols and full curve,* Fig. 5).

GENERAL DISCUSSION

Surface plasmon-optical methods as well as neutron reflection techniques are both well established for the characterization of ultrathin organic films like polymer coatings or lipid monolayers. In this study, for the first time, a systematic comparison between both experimental approaches is reported for the interfacial recognition and binding reaction between streptavidin and biotin at a solid-solution interface. This was possible because both techniques can be applied in a total internal reflection geometry, thus allowing for the investigation of identical sample configurations.

Despite the fact that the two techniques are sensitive to different physical properties, the structural data obtained from both experiments are in satisfying agreement (cf. Table 3). On the other hand, this is not too surprising because both data sets monitor in a similar way only sample properties that vary normal to the plane of the layer architecture with no attention to lateral resolution. The analysis of the reflectivity data in both cases yields thickness data with Ångstrom resolution averaging in the plane of the layer over the whole probe beam (several cm^2 for neutrons and mm^2 for the laser experiments). Since for our sample the relative contrasts between the substrate, the lipid layers, and the protein layers are similar in both cases, the obtained sensitivities are comparable.

Clearly, the optical technique is much easier to apply and can be installed in a normal laboratory with relatively simple equipment. The neutron reflection technique, however, bears the potential advantage of generating contrast between sublayers in a complex interfacial architecture by selectively deuterating individual units in the supramolecular assembly.

To demonstrate this, we performed a series of simulations with different layers being fully deuterated. The various configurations and the calculated reflectivity curves are presented in Fig. 6. In each of the hypothetical

TABLE 3 Neutron and optical reflectivity data used to fit the respective experimental curve obtained after streptavidin binding to the biotin-functionalized lipid layers (cf. Figs. 3, 4, and 5)

Sample	Thickness	Scattering length density
Neutron data	8.1 ± 0.5 nm	$2.32 \cdot 10^{-4}$ nm^{-2} (x = 38% D_2O)
Three CdA		
Biotinylated lipid monolayer d_1	[1.7 nm]*	$2.74 \cdot 10^{-4}$ nm^{-2} (x = 43% D_2O)
Streptavidin d_2	[4.1 nm]*	$3.09 \cdot 10^{-4}$ nm^{-2} (x = 30% D_2O)
$d_1 + d_2$	5.8 nm*	
Sample	**Thickness**	**Index of refraction**
Optical data		
LaSFN9		n = 1.846
Au layer	d = 44.7 nm	$\tilde{\epsilon} = 12.0 + i \cdot 1.25$
SiO_x layer	d = 4.5 nm	n = 1.45
Three CdA layer	d_0 = 8.3 nm	n = 1.50
Biotinylated DPPC d_1	d_1 = 3.1 nm	n = 1.50
Streptavidin d_2	2.8 nm	n = 1.45
$d_1 + d_2$	5.9 nm	

* The bracket for the thickness values of the biotinylated lipid monolayer d_1 and of the streptavidin layer d_2, respectively, indicates the somewhat arbitrary choice. Only the sum of the two layers can be determined.

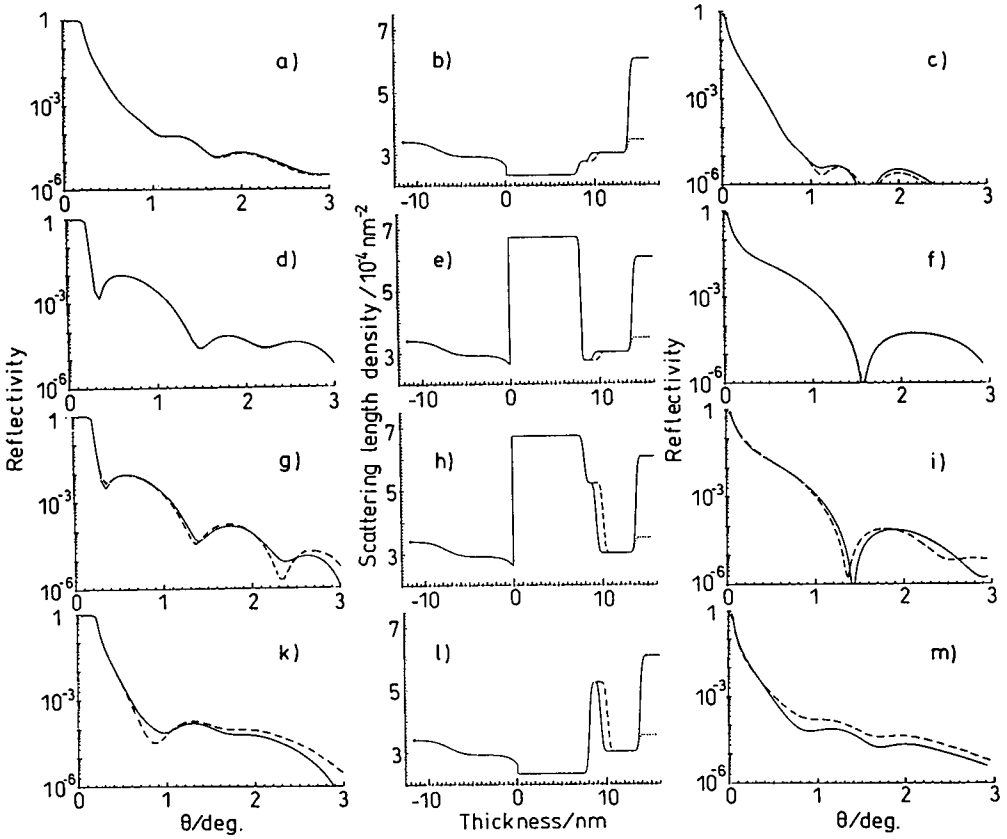

FIGURE 6 Series of reflectivity simulations for sample architectures each consisting of a quartz substrate/three layers of CdA/one layer of biotinylated lipid/one layer protein, but with different combinations of protonated and deuterated molecules and hence different scattering length densities. *b* and *l* are with protonated CdA, *e* and *h* with deuterated CdA; *b* and *e* use protonated lipid, *h* and *l* deuterated lipid. The reflectivity curves in the left panel (*a*, *d*, *g*, and *k*) are calculated with D_2O in the aqueous medium (*full lines* in *b*, *e*, *h*, and *l*), those given in the right panel (*c*, *f*, *i*, and *m*) with H_2O (*dotted lines* in the *middle panel*). For each reflectivity curve, two examples are given (as *full* and *dashed curve*, respectively), demonstrating the difference as obtained by varying the lipid layer thickness from 1.3 to 2.1 nm, but keeping the sum of the thicknesses for lipid and protein layer (5.8 nm) constant.

sample architectures, the following layers were included: quartz substrate with its specific scattering length density profile at the surface; three layers of CdA (d = 8.1 nm), either protonated (*b* and *k*) or deuterated (*e* and *h*); one layer of biotinylated lipid, either protonated (*b* and *e*) or deuterated (*h* and *k*); one layer of protein (protonated). The aqueous phase was either D_2O (*full line* in *b*, *e*, *h*, and *k*) with the reflectivity curves given in the left panel (*a*, *d*, *g*, and *j*) or H_2O (*dotted curves* and right panel, *c*, *f*, *i*, and *l*). In each case, the sum of the thicknesses of the biotinylated lipid and the protein layer was kept constant at d = 5.8 nm. In one series of simulations, however, the lipid layer was fixed at a thickness of d_1 = 1.3 nm (*full curve* in each of the reflectivity plots) in a second series at d_2 = 2.1 nm (*dashed curves*).

The configuration employed in our studies corresponds to Fig. 6 *b* with D_2O as aqueous medium. As discussed above, there is no possibility to discriminate between the thickness of lipid or protein layer (cf. Fig. 6 *a, dashed and full curve*). The use of H_2O would have generated a slight difference between the two reflectivity curves (cf. Fig. 6 *c*), however, at an intensity level of the reflected neutron beam ($R = 10^{-6} \cdots 10^{-5}$) not accessible with standard instruments. As is demonstrated in Fig. 6, *d–f*, the use of deuterated CdA buffer layers would not have generated any contrast that would have allowed one to measure more accurately the contributions of lipid and protein layer, respectively. The comparison between *c* and *f*, nevertheless, demonstrates the tremendous effect of CdA deuteration on the overall reflectivity curve leading to a difference in the reflected intensities of up to two orders of magnitude (e.g., at $\theta = 0.1°$). This might be helpful in other studies where the CdA layers are replaced by polymeric buffer systems.

The situation changes significantly by using in addition to the deuterated CdA layers also a deuterated lipid layer (cf. Fig. 6 *h*). Now for both D_2O and H_2O (cf. Fig. 6, *g* and *i*, respectively) in the aqueous phase, a pronounced difference of the two reflectivity curves is found; however, again at an intensity level dominated by the statistical noise in the data and therefore not useful. The really interesting case is the one presented in Fig. 6 *l*). Only the biotin-lipid monofilm is deuterated and hence shows a large contrast to its neighboring layers. Its thickness varia-

tions now lead to a measurable difference in the reflectivity curves at accessible intensity levels with significant differences in D_2O (Fig. 6 *k*) and H_2O (Fig. 6 *m*), respectively.

Such a system now can be investigated by neutron reflectivity measurement even with respect to its internal structure. This unique feature of the technique certainly justifies the cost and effort of neutron experiments, in particular, if complemented by optical measurements.

Helpful discussions with F.-J. Schmitt, R. Blankenburg, M. Lösche, and H. Ringsdorf are gratefully acknowledged. We are indebted to B. Diederich for her help with the TOREMA experiments, to G. Reiter and M. Stamm for their contributions related to neutron reflectivity data evaluation, and to M. Liley for performing fluorescence microscopic experiments.

Financial support came from the Bundesministerium für Forschung und Technologie (O3 KN2MPG) and from Boehringer Mannheim GmbH, Werk Tutzing.

Received for publication 12 November 1991 and in final form 13 March 1992.

REFERENCES

1. Green, N. M. 1975. Avidin. *In* Advances in Protein Chemistry. M. C. Anson and J. T. Edsell, editors. Academic Press, New York. 85–133.
2. Wilchek, M., and E. A. Bayer. 1990. Avidin-biotin technology. *In* Methods in Enzymology. Vol. 184. Academic Press, New York. 5–51.
3. Blankenburg, R., P. H. Meller, H. Ringsdorf, and C. Salesse. 1989. Interaction between biotin lipids and streptavidin monolayers: formation of oriented two-dimensional protein domains induced by surface recognition. *Biochemistry.* 28:8214–8221.
4. Schmitt, F.-J., A. L. Weisenhorn, P. K. Hansma, and W. Knoll. 1991. Interfacial recognition reactions as seen by fluorescence-, surface plasmon-, and atomic force microscopies. *Makromol. Chem. Macromol. Symp.* 46:133–143.
5. Taylor, D. M., H. Morgan, and C. D'Silva. 1991. Assembling Networks for Molecular Electronics. *Makromol. Chem. Macromol. Symp.* 46:1–8.
6. Schmitt, F.-J., and W. Knoll. 1991. Surface-plasmon microscopic observation of site-selective recognition reactions. *Biophys. J.* 60:716–720.
7. Helm, C. A., W. Knoll, and J. Israelachvili. 1991. Measurement of ligand-receptor interactions. *Proc. Natl. Acad. Sci. USA* 88:8169–8173.
8. Häussling, L., H. Ringsdorf, F.-J. Schmitt, and W. Knoll. 1991. Biotin-functionalized self-assembled monolayers on gold: surface plasmon optical studies of specific recognition reactions. *Langmuir* 7:1837–1840.
9. Morgan, H., D. M. Taylor, C. D'Silva, and H. Fukushima. 1992. Self-assembly of streptavidin/bisbiotin monolayers and multilayers. *Thin Solid Films.* 210/211: 773–775.
10. Herron, J. N., W. Müller, M. Paudler, H. Riegler, H. Ringsdorf, and P. A. Suci. 1992. Specific recognition-induced self-assembly of a biotinlipid/streptavidin/Fab-fragment triple layer at the air/water interface: ellipsometry and fluorescence microscopy investigations. *Langmuir* 8:1413–1416.
11. Vaknin, D., J. Als-Nielsen, M. Piepenstock, and M. Lösche. 1992. Recognition processes at a functionalized lipid surface observed with molecular resolution. *Biophys. J.* In press.
12. Schmitt, F.-J. 1991. Ph.D. thesis. Specific protein adsorption at functionalized interfaces. Universität Mainz, Germany.
13. Kuhn, H., D. Möbius, and H. Bücher. 1972. Spectroscopy of monolayer assemblies. *In* Physical Methods of Chemistry. A. Weissberger and B. W. Rossiter, editors. Wiley, New York.
14. Knoll, W. 1991. Optical characterization of organic thin films and interfaces with evanescent waves. *MRS Bulletin.* 16:29–39.
15. Als-Nielsen, J., and K. Kjaer. 1989. X-ray reflectivity and diffraction studies of liquid surfaces and surfactant monolayers. *In* Phase Transitions in Soft Condensed Matter. T. Riste and D. Sherrington, editors. Plenum Press, New York. 113–138.
16. Raether, H. 1988. Surface plasmons on smooth and rough surfaces and in gratings. Springer Tracts in Modern Physics. Vol. 111. Springer Verlag, Berlin. 136 pp.
17. Stamm, M., G. Reiter, and S. Hüttenbach. 1989. A neuron reflectometer for the investigation of solids and liquid interfaces. *Physica B* 156/157:564–566.
18. Lekner, J. 1987. Theory of reflection. Martinus Nijhoff Publications, Dordrecht, The Netherlands. 364 pp.
19. Kretschmann, E. 1972. Die Bestimmung optischer Konstanten von Metallen durch Anregung von Oberflächenplasmaschwingungen. *Z. Physik* 241:313–324.
20. Jark, W., G. Comelli, T. P. Russel, and J. Stöhr. 1989. Structural studies of Langmuir-Blodgett multilayers by means of soft X-ray diffraction. *Thin Solid Films.* 170:309–319.
21. Büldt, G., H. U. Gally, A. Seelig, J. Seelig, and G. Zaccai. 1978. Neutron diffraction studies on selectively deuterated phospholipid bilayers. *Nature (Lond.)* 271:182–184.
22. Schmidt, G., and W. Knoll. 1985. Densitometric characterization of aqueous lipid dispersions. *Ber. Bunsen-Ges Phys. Chem.* 89:36–43.
23. Bayerl, T. M., R. K. Thomas, J. Penfold, A. Rennie, and E. Sackmann. 1990. Specular reflection of neutrons at phospholipid monolayers: changes of monolayer structure and headgroup hydration at the transition from the expanded to the condensed phase state. *Biophys. J.* 57:1095–1098.
24. Helm, C. A., H. Möhwald, K. Kjaer, and J. Als-Nielsen. 1987. Phospholipid monolayer density distribution perpendicular to the water surface. A synchrotron X-ray reflectivity study. *Europhys. Lett.* 4:697–703.
25. Swalen, J. D. 1986. Optical properties of Langmuir-Blodgett films. *J. Mol. Electron.* 2:155–181.
26. Kooyman, R. P. H., and U. J. Krull. 1991. Surface plasmon microscopy of two crystalline domains in a lipid monolayer. *Langmuir* 7:1506–1509.
27. Hendrickson, W. A., A. Pähler, J. L. Smith, Y. Satow, E. A. Merritt, and R. P. Phizackerley. 1989. Crystal structure of core streptavidin determined from multiwavelength anomalons diffraction of synchrotron radiation. *Proc. Natl. Acad. Sci. USA.* 86:2190–2194.
28. Morgan, H., D. M. Taylor, and C. D'Silva. 1992. Surface plasmon resonance studies of chemisorbed biotin-streptavidin multilayers. *Thin Solid Films.* 209:122–126.